COMPREHENSIVE FINAL REPORT FOR CDFA AGREEMENT NUMBER 16-0510-SA: CHARACTERIZATION OF *XYLELLA FASTIDIOSA* PLANT CELL WALL DEGRADATION AND INHIBITION OF THE TYPE II SECRETION MACHINERY

Principal Investigator
Caroline Roper
Dept. Microbiology and Plant Pathology
University of California
Riverside, CA 92521
mcroper@ucr.edu

Co-Principal Investigator
Dario Cantu
Dept. of Viticulture and Enology University of California
Davis, CA 95616
dacantu@ucdavis.edu

Co-Principal Investigator
Andrew McElrone
USDA-ARS, Dept. Viticulture and Enology University of California
Davis, CA 95616
ajmcelrone@ucdavis.edu

Co-Principal Investigator
Qiang Sun
Department of Biology
University of Wisconsin Stevens Point, WI 54481
Qiang.Sun@uwsp.edu

Cooperator
John Labavitch
Dept. of Plant Sciences
University of California Davis, CA 95616
jmlabavitch@ucdavis.edu

Reporting Period: The results reported here are from work conducted July 2016 to February 2019.

INTRODUCTION

Xylella fastidiosa (*Xf*) is the causal agent of Pierce's Disease (PD) of grapevine, a serious and often lethal disease (Hopkins and Purcell, 2002, Chatterjee et al., 2008, Purcell and Hopkins, 1996). This xylem-limited bacterial pathogen colonizes the xylem and in doing so must be able to move efficiently from one xylem vessel element to adjacent vessels (Roper et al. 2007). Xylem conduits are separated by pit membranes (PMs) that are composed of primary cell wall and serve to prevent movement of air embolisms and pathogens within the xylem (Buchanan, 2000). More specifically, PMs are composed of cellulose microfibrils embedded in a meshwork of pectin and hemicellulose (Buchanan, 2000). The pore sizes within that meshwork range from 5 to 20 nM, which will not allow passive passage of *Xf* cells whose size is 250-500 x 1,000-4,000 nM (Perez-Donoso et al., 2010, Mollenhauer & Hopkins, 1974). Based on functional genomics and *in planta* experimental evidence, *Xf* utilizes cell wall-degrading enzymes (CWDEs) to actively digest the polymers within the PMs, thereby facilitating its movement throughout the xylem network (Simpson et al. 2000, Roper et al., 2007, Perez-Donoso et al., 2010). It is known that polygalacturonase (PG) is a major pathogenicity factor for *Xf* (Roper et al., 2007) and that it acts in concert with at least one EGase to breach the PM barrier (Perez-Donoso et al. 2010). EGases are implicated in virulence and colonization of the xylem in other bacterial phytopathogens, such as *Pantoea stewartii* subsp. *stewartii*, *Ralstonia solanacearum* and *Xanthomonas campestris* pv. *campestris* (Gough, 1988, Roberts et al., 1988, Saile et al., 1997, Mohammadi et al., 2012). In our previous study (project # 14-0144-SA), we tested the role of the *Xf* EGases *in planta* by constructing deletion mutants in two of the EGases (Δ*engXCA1* and Δ*engXCA2*) and mechanically inoculating the modified *Xf* lines into *Vitis vinifera* cv. Cabernet sauvignon and cv. Chardonnay grapevines.

PD symptom development is tightly correlated with the ability of *Xf* to degrade specific polysaccharides, namely fucosylated xyloglucans (part of the hemicellulosic component) and weakly esterified homoglacturonans (part of the pectin portion), that make up the intervessel PMs (Sun et al., 2011). In general, pectin is one of the first targets of cell wall digestion for invading pathogens and the resulting oligogalacturonides (OGs), which are smaller pieces of the pectin polymer, that are released are likely used as a carbon source for the invading pathogen. In addition, specific OGs with a degree of polymerization in the size range of 10-15 residues can also serve as signals that trigger host defense responses (Benedetti et al., 2015). These responses include accumulation of reactive oxygen species (ROS), expression of pathogenesis-related proteins, deposition of callose, activation of mitogen-activated protein kinases (MAPKs), among other defense related processes (Boller & Felix, 2009, Benedetti et al., 2015).

Tyloses are outgrowths of parenchyma cells that emerge through vessel-parenchyma pits into vessel lumen, and are common in a wide range of species (Bonsen and Kučera 1990; Esau 1977; Tyree and Zimmermann 2002). Tyloses impede fluid penetration (Parameswaran et al. 1985) and induce a permanent state of reduced hydraulic conductivity, and are triggered by abiotic and biotic stresses, such as pathogen infection (Aleemullah and Walsh 1996; Collins et al. 2009; Dimond 1955; Parke et al. 2007). Tylose formation is the predominant vascular occlusion associated with *Xf* infection (Fig 1A, B), and excessive tylose development has been linked to the extreme susceptibility of *Vitis vinifera* wine grapes to PD (Fritschi et al. 2008; Sun et al. 2013).

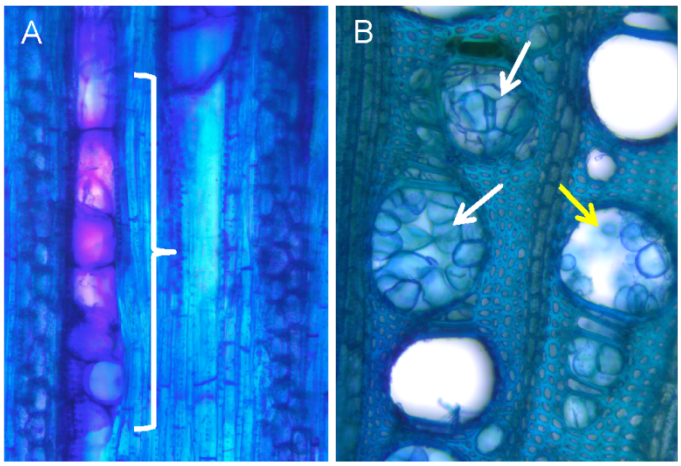

Figure 1: Xylem vessels of *V. vinifera* grapevines inoculated with *Xf*. A) Longitudinal section B) cross-section. Grapevine petiole sections were stained with toluidine blue O (0.05%). White arrows and bracket indicate vessels that are completely occluded with tyloses, and yellow arrow indicates a partially occluded vessel. Images taken by J. Rapicavoli (Roper Lab).

Importantly, rates of tylose development in *V. arizonica*, a resistant species, are much lower than those in *V. vinifera*, which may reflect differing innate immune responses to the presence of *Xf* in the xylem. To our knowledge, there is little knowledge of the molecular mechanisms underlying the differences in response to *Xf* among different *V. vinifera* cultivars. Thus, we sought out to better understand this difference in cultivar response to *Xf* in the context of host cell wall degradation and the elicitation of specific defense responses that lead to tylose formation in grapevines. Interestingly, a preliminary analysis of tylose formation in Cabernet Sauvignon vines inoculated with the Δ*engXCA1* mutant using a high resolution microCT technique (X-ray micro-computed tomography) by the McElrone laboratory determined that these vines exhibited fewer tyloses than those inoculated with wild type *Xf* (Fig. 2). Therefore, our hypothesis is that enzymatic degradation of the plant cell wall by *Xf* CWDEs is generating cell wall fragments that elicit DAMP signaling defense pathways, which leads to downstream tylose production and PD symptom development in certain grape cultivars.

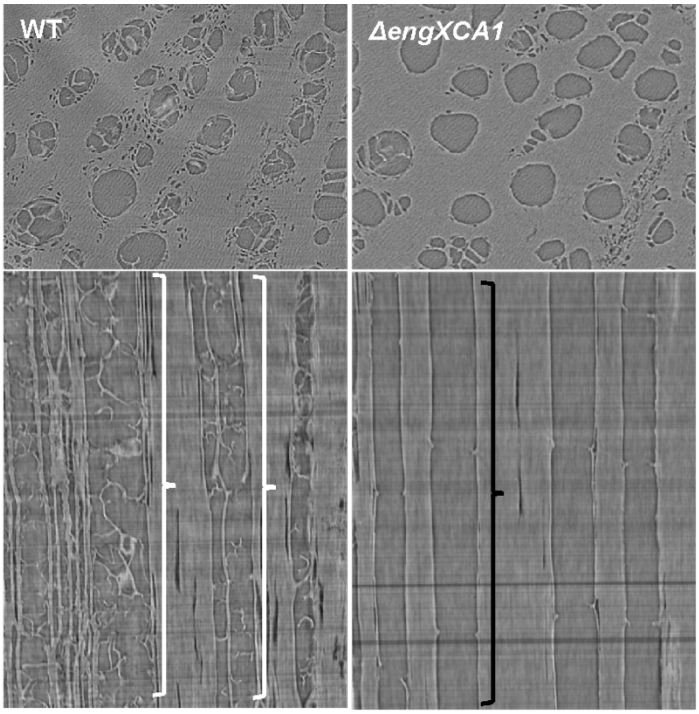

Figure 2: Images of grapevine xylem vessels obtained using microCT. Vines inoculated with wild-type Temecula 1 *Xf* had substantial vascular occlusions, whereas vines inoculated with Δ*engXCA1* had few tyloses similar to the PBS negative control (not shown). Top panels are cross-sectional views and bottom panels are longitudinal views. White brackets highlight occluded vessels and black bracket highlights open vessel.

OBJECTIVES

1) Qualitative analysis of the effect of cell wall degradation on the grapevine response to *Xf*.
2) Quantitative analysis of plant defense pathways induced by *Xf* cell wall degrading enzyme activity: biochemical and transcriptional studies.
3) Inhibition of the Type II secretion system using natural products produced by grapevine microbial endophytes.

DESCRIPTION OF ACTIVITIES

Qualitative analysis of the effect of cell wall degradation on the grapevine response to *Xf*.

In the context of plant cell wall degradation, we are examining the effects that different *Xf* mutants (Δ*engXCA1*, Δ*engXCA2*, *egl* (all EGases and EGase/expansin hybrid) and *pglA* (a PG)) have on integrity and carbohydrate composition of grapevine pit membranes in different varieties using both microscopic and immunological techniques coupled with fluorescence (Sun et al., 2011) and/or electron (Sun et al., 2017) microscopy.
We are coupling these microscopic observations with macroscopic studies of the spatial distribution of tyloses and other vascular occlusions, such as plant-derived gels and bacterial aggregates using high resolution micro-computed tomography (microCT). This non-destructive method technique uses x-rays to create cross-sections of an object that can be used to re-create a virtual model (3D model). These experiments will allow us to match degradation of specific host cell wall carbohydrates with spatiotemporal patterns of production of tyloses in 3 dimensions.

Xf wildtype and mutant strains (Δ*engXCA1,* Δ*engXCA1,* Δ*engXCA1*/Δ*engXCA2,* Δ*pglA and* Δ*egl)* have been used to inoculate Cabernet Sauvignon and Chardonnay grapevines in the greenhouse. PBS-inoculated vines were used as negative controls. Each *Xf* strain was inoculated into 27 plants (3 biological replicates with 9 technical replicates each) and PD symptoms were rated each week using the 0 – 5 PD rating index (Guilhabert and Kirkpatrick, 2005). Vine tissue samples are currently being collected for each of the three experiments: stem and petiole tissue for RNAseq, stem tissue for microCT analysis, and stem explants for EM analysis. Samples from three biological replications (consisting of three technical replications) per treatment have been collected at two

time-points covering early and mid-infection based on the PD rating index (Early infection = 1 – 2, Mid-infection = 2 – 3) and are currently being analyzed or awaiting analysis.

Modifications of different *Xf* strains on xylem structures of Chardonnay vines--Chardonnay vine samples from early and late timepoint were analyzed using scanning electron microscopy to study vascular occlusion, pit membrane integrity and presence/absence of *Xf* in the xylem tissue after inoculation. Samples were inoculated with PBS and all or most of the following *Xf* genotypes: Temecula 1, Fetzer 1, Δ*engXCA1*, Δ*engXCA1/XCA2,* Δ*egl* and Δ*pglA*. PBS inoculated samples are used as negatively controls while *Xf* wild types (Temecula 1 and Fetzer 1)-inoculated samples as positive controls.

Our results have indicated that no vascular occlusions (Fig. 3) were present in both the early (Fig. 3A, B) and late (Fig. 4C, D) timepoint samples from the vines inoculated with PBS. *Xf* cells were not observed either in the samples. Intervessel PMs were intact in the samples from early timepoint and were also mostly intact in those from the late timepoint.

Chardonnay vines inoculated with wild-type Temecula 1 showed very different structural features in the secondary xylem between samples from the early timepoint (Fig. 4A, B) and those from the late timepoint (Fig. 4C, D). In the samples from the early timepoint, secondary xylem contained no or very few vessels with tyloses (Fig. 4A). In contrast, most vessels in the samples from the late timepoint were completely occluded by tyloses (Fig. 4C). Vessel parenchyma PMs were intact with a mostly smooth surface in the samples from either timepoint, but broken intervessel PMs were present to different extents with low frequencies in the early-timepoint samples (Fig. 5B) but a very high frequency from the late-timepoint samples (Fig.4D). Either very porous intervessel PMs or the lack of intervessel PMs from intervessel pits was common in the samples from the late timepoint. *Xf* cells were seldom seen in the xylem from the early timepoint, but commonly occurred in the vessels with broken intervessel PMs (Fig. 4D).

In the vines inoculated with wild-type Fetzer, a majority of vessels in the samples from the late timepoint were occluded by tyloses (Fig. 5A, B). Some vessel-parenchyma PMs had a relatively rough surface while a small number of intervessel PMs were obviously degraded (Fig. 5C).

Xylem tissues in Chardonnay vines from the early and late timepoint inoculated with Δ*engXCA1 Xf* had some different features (Fig. 6). Occlusion was present in very few vessels in the samples from the early timepoint (Fig. 6A) but in a moderate number of vessels in those from the late timepoint (Fig. 6D). Tyloses forming the occlusions were small and did not fill up the vessels that contained them in the samples from the early timepoint (Fig. 6B), but were mostly fully developed, completely occluding the vessels with them in those from the late timepoint (Fig. 6E). Most intervessel PMs were intact in the samples from the early timepoint although cracks were visible in few intervessel PMs (Fig. 6C) while a moderate number of intervessel PMs were degraded with very porous PMs in the samples from the late timepoint (Fig. 6F). *Xf* cells were observed in the samples from either timepoint (Fig. 6C).

Samples of Chardonnay vines from the late timepoint inoculated with Δ*engXCA1*/*ΔengXCA2* (Fig. 7) and Δ*egl* (Fig. 8), respectively were also examined. In both types of samples, xylem contained a majority of open vessels and very few vessels were observed to have tyloses. Tyloses in the few vessels were mostly at the early developmental stages in the samples inoculated with Δ*engXCA1*/*ΔengXCA2 Xf* (Fig. 8A), but were fully developed and occurred as patches in those with Δ*egl Xf* (Fig. 8A, B). *Xf* cells were observed in the samples inoculated with either *Xf* mutant (Fig. 8B). Although very porous intervessel PMs were observed in the samples with Δ*engXCA1*/*ΔengXCA2 Xf*, a majority of intervessel PMs maintained some degrees of integrity with a relatively rough surface with small irregular cracks (Fig. 7B).

In the samples of Chardonnay vines from the early timepoint inoculated with Δ*pglA,* no occluded vessels were seen in the secondary xylem (Fig. 9A, B). Intervessel PMs had a smooth surface without visible pores and broken intervessel PMs were absent or rare (Fig. 9C). *Xf* cells were not observed in the samples examined.

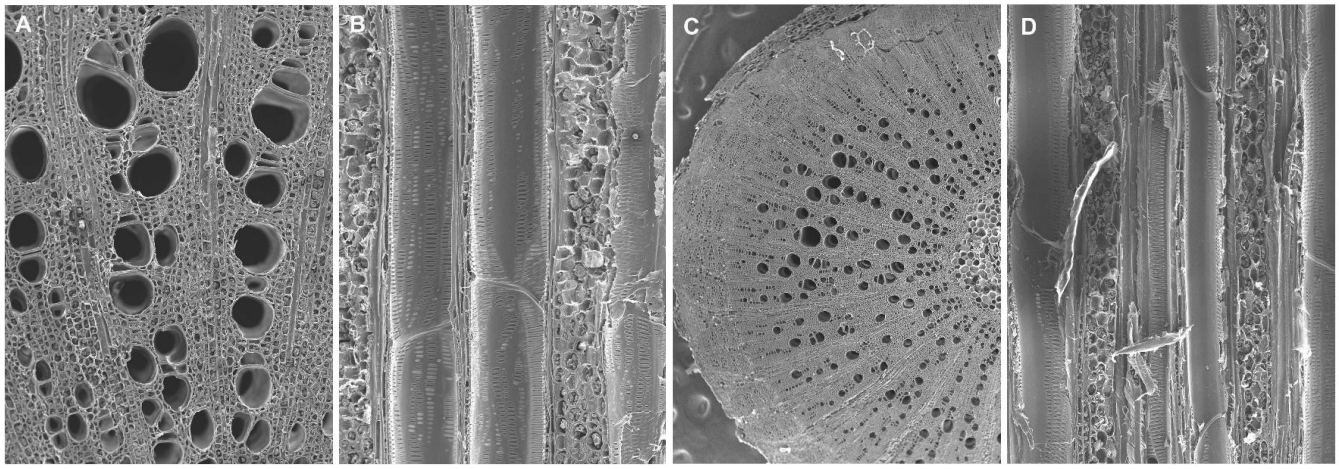

Figure 3: Xylem tissue in Chardonnay vines inoculated with PBS at early (A and B) and late (C and D) timepoint. **A and C.** Transverse section of secondary xylem showing absence of vascular occlusion in the vessels. **B and D.** Tangential longitudinal section of secondary xylem, showing transected vessels that have intact vessel-parenchyma PMs and do not contain vascular occlusions.

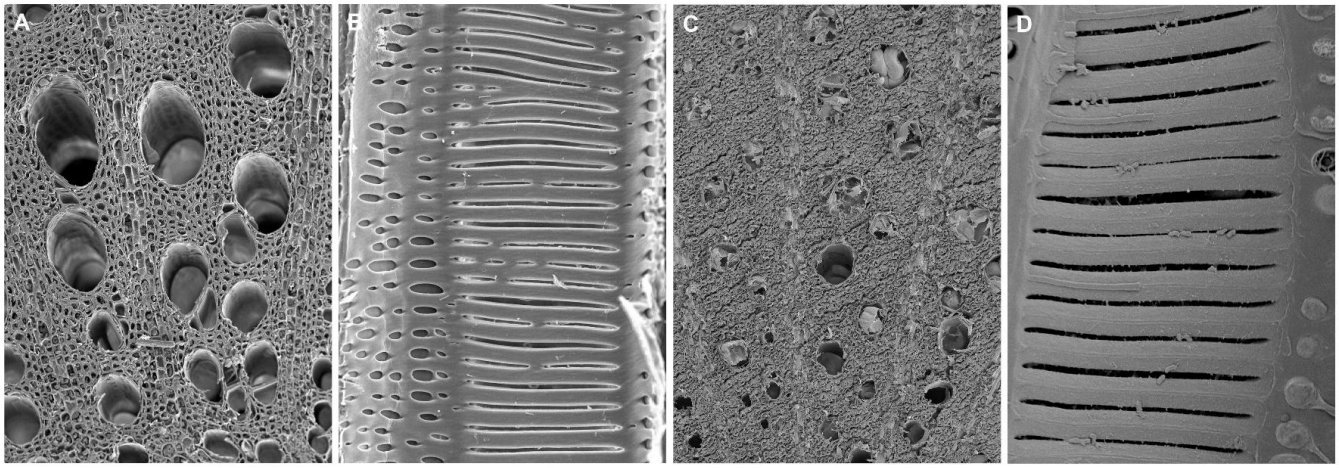

Figure 4: Xylem tissue of Chardonnay vines inoculated with wild-type Temecula 1 from the early (A and B) and late (C and D) timepoint. **A** and **C.** Transverse section of secondary xylem. **B** and **D**. Tangential longitudinal section of secondary xylem. **A**. Open vessels in xylem tissue. **B**. Intact oval-shaped vessel-parenchyma PMs and broken scalariform intervessel PMs seen through the pit apertures. **C**. Most vessels are completely occluded by tyloses. **D**. Intervessel PMs disappeared from their original places and *Xf* cells were present.

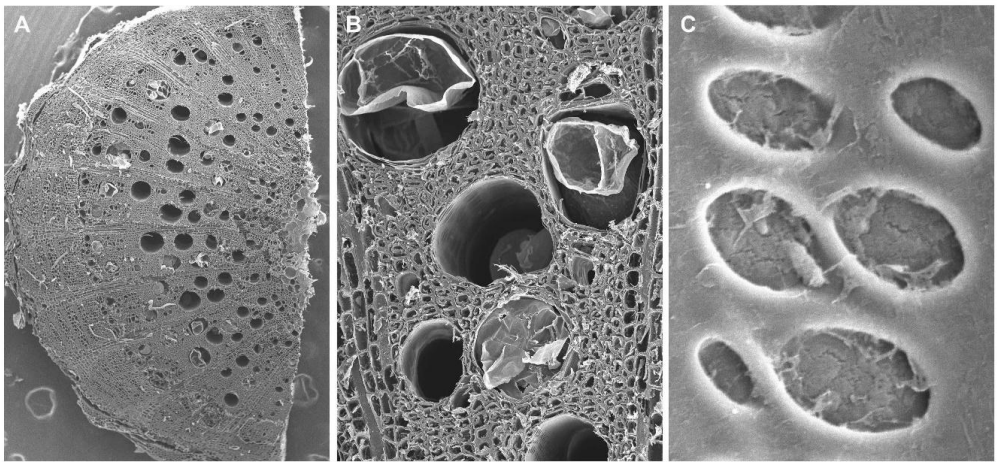

Figure 5: Xylem tissue of Chardonnay vines inoculated with wild-type Fetzer from the late timepoint. **A and B.** Transverse section of secondary xylem. **A.** Occurrence of vascular occlusion in an abundant number of vessels. **B.** Vessels are occluded by tyloses. **C.** A transected vessel, showing oval vessel-parenchyma pit pairs, rough vessel-parenchyma PM surface and *Xf*

cells.

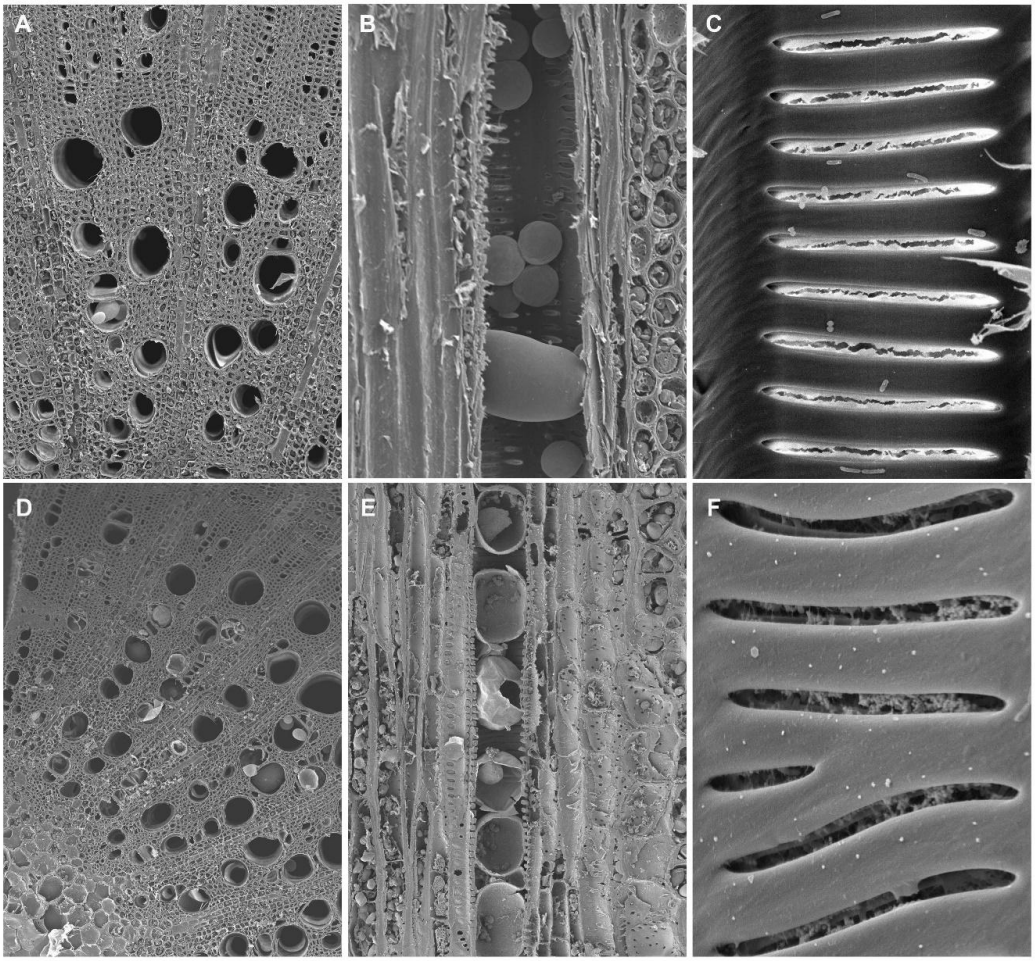

Figure 6: Xylem tissue of Chardonnay vines inoculated with *ΔengXCA1 Xf* from the early (**A-C**)- and late (**D-F**) timepoint. **A** and **D**. Transverse section of xylem tissue. **B**, **C**, **E** and **F**. Tangential longitudinal section of xylem tissue. **A**. Very few vessels are occluded. **B**. A vessel containing tyloses at their early developmental stages. **C**. a crack/cracks in intervessel PMs and *Xf* cells in the vessel. **D**. a moderate number of vessels are occluded. **E**. One occluded vessel is filled up with fully developed tyloses. **F**. Very porous intervessel PMs seen through pit apertures. *ΔengXCA1 Xf* are present on the lateral wall.

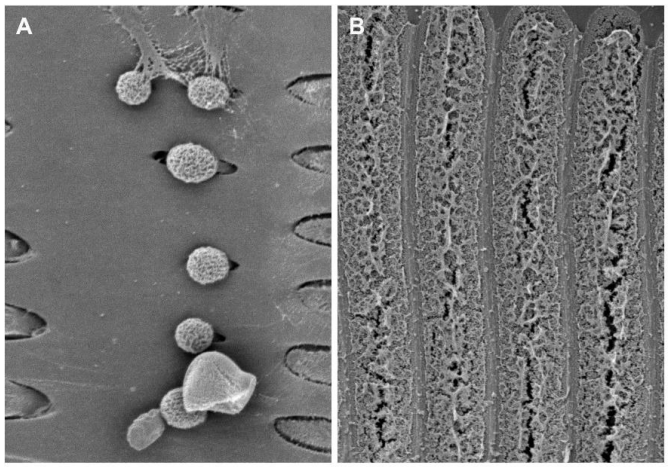

Figure 7: Xylem tissue of Chardonnay vines inoculated with *ΔengXCA1/ ΔengXCA2 Xf* from the late timepoint. **A**. Tangential longitudinal section of secondary xylem, showing very small tyloses developing from vessel-parenchyma pit pairs. B. Tangential longitudinal section of secondary xylem, showing intervesssel PMs with a rough surface and small cracks.

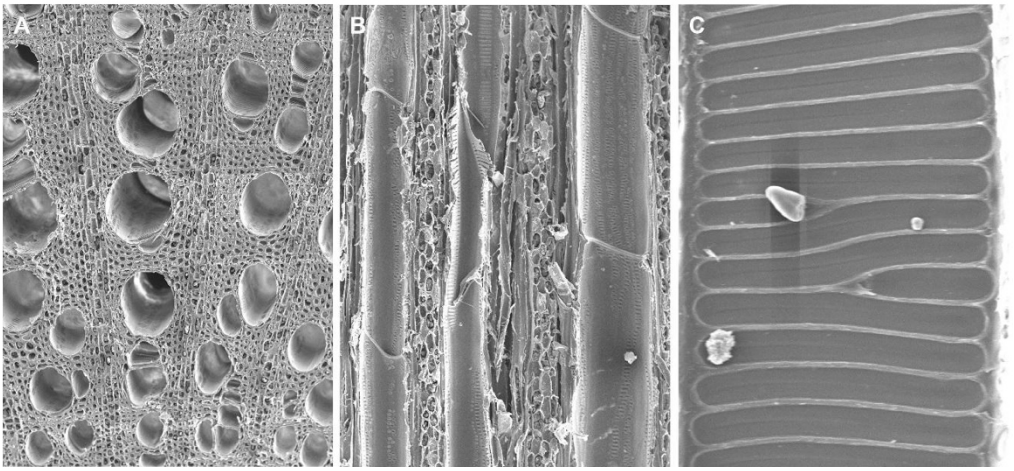

Figure 8: Xylem tissue of Chardonnay vines inoculated with *ΔpglA* from the early timepoint. **A.** Transverse section of secondary xylem. All the vessels are free of vascular occlusion. **B.** Tangential longitudinal section of secondary xylem, showing several transected vessels without vascular occlusion. **C.** Tangential longitudinal section, showing intact intervessel PMs with a smooth surface on a vessel's lateral wall.

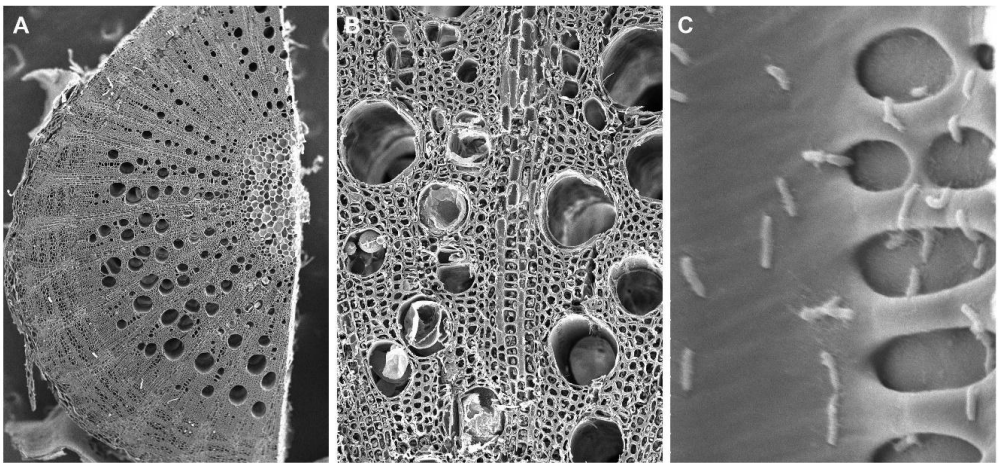

Figure 9: Xylem tissue of Chardonnay vines inoculated with *Δegl Xf* from the late timepoint. **A** and **B**. Transverse section of secondary xylem. **A.** A majority of vessels are open and very few occluded vessels occurred in a patch. **B.** vessels with occlusion are mostly completely filled up by tyloses. **C.** *Xf* cells are present in a vessel.

Modifications of different *Xf* strains on xylem structures of Cabernet Sauvignon vines-We examined some late timepoint stem samples of Cabernet Sauvignon vines that were inoculated with PBS, wild-type *Xf* strains (Temecula 1 and Fetzer) and mutant *Xf* strains (Δ*engXCA1*, Δ*engXCA2*, Δ*engXCA1*/*engXCA2*, Δ*egl* and Δ*pglA*), respectively. We found that at the late time-point of PD symptom development, certain *Xf* strains display differences in vascular occlusion, intervessel PM integrity and *Xf* existence at the third internode above the point of inoculation. Some preliminary data from the middle time-point are also included here to explore the process of xylem structure modifications during PD symptom progression. The remaining samples from the mid and late timepoints are still being analyzed as well as the early timepoint.

In the vines inoculated with PBS, vascular occlusion and *Xf* cells were not observed in the secondary xylem at both middle (Fig. 10) and late (Fig. 11) time-point. Intervessel PMs observed remained intact at the middle time- point but broken PMs were seen in a few vessels in the samples of the late timepoint.

The inoculation with wild-type *Xf* also caused significant xylem structural modifications in Cabernet Sauvignon vines. At the middle time-point, about 30% of the vessels in the transverse section of secondary xylem

contained tyloses (Fig. 12A), which partially or completely occluded the vessels (Fig. 12B). Wild-type *Xf* cells were also present in many vessels and occurred individually (Fig. 13C) or as small clusters (Fig. 13D). At the late timepoint, over 50% of the vessels in the transverse section of a stem were occluded by tyloses and *Xf* cells occurred as large clusters in addition to individual occurrence or small clusters (Fig. 14A). Moderate amounts of degraded intervessel PMs were observed in both the middle and late time-point samples (Figs. 12C and 13B).

In Δ*engXCA2*-inoculated Cabernet Sauvignon vines, vascular occlusion occurred in a small extent at the middle time-point (Fig. 14A and B) and increased in quantity at the late time-point with the occluded vessels making up about 30 % of the total vessels (Fig. 15A and B). Δ*engXCA2* cells were present in the samples of both time-points (Fig. 14C and 15C, D). There are more broken intervessel PMs at the late time-point (Fig. 15C and D) than at the middle time-point (Fig. 14C). However, the inoculation with Δ*engXCA1* resulted in little or no vascular occlusion in the samples of the late time-point (Fig. 16A). Some degrading intervessel PMs with different porosities were also seen in the Δ*engXCA1*-infected samples at the late time-point (Fig. 16B and C). Interestingly, in the late time-point samples inoculated with the Δ*engXCA1*/*engXCA2* double mutant, tyloses were absent or occurred in very few vessels (Fig. 17A and B) and Δ*engXCA1*/*engXCA2* cells were not observed (Fig. 17C). Intervessel PMs were mostly intact despite the existence of degrading intervessel PMs in few vessels (Fig. 17D).

The inoculation with Δ*egl* also caused occlusion of a moderate number of vessels in the infected Cabernet Sauvignon vines at the late time-point (Fig. 18A and B). Δ*egl* cells were abundantly present in some vessels and broken intervessel PMs in few vessels (Fig. 18C).

In the Fetzer-inoculated late time-point samples, most vessels were free of occlusions (Fig. 20A) and tyloses present in few vessels were at early developmental stages and did not occlude the vessels (Fig. 20D). Fetzer cells and broken intervessel PMs were present only in few vessels (Fig. 20C). Similarly, in the Δ*pglA*-inoculated samples, vessels were almost free of occlusions (Figs. 19A, B and 21B) and broken intervessel PMs (Fig. 19C) were seen in few vessels at both middle time-point and late time-point (Fig. 20B). Δ*pglA* cells were not observed in either of the timepoints (Fig. 19C).

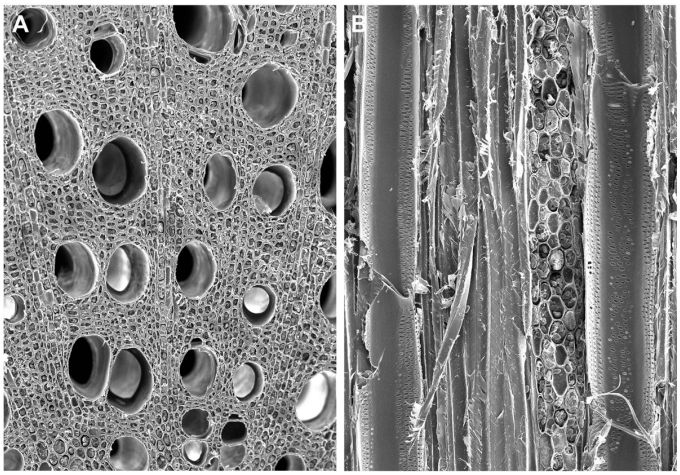

Figure 10: Xylem structural features in PBS-inoculated Cabernet Sauvignon vine at the middle time-point. **A.** Transverse section of secondary xylem. All the vessels are free of vascular occlusions. **B.** Tangential longitudinal section of secondary xylem showing two transected vessels without vascular occlusions.

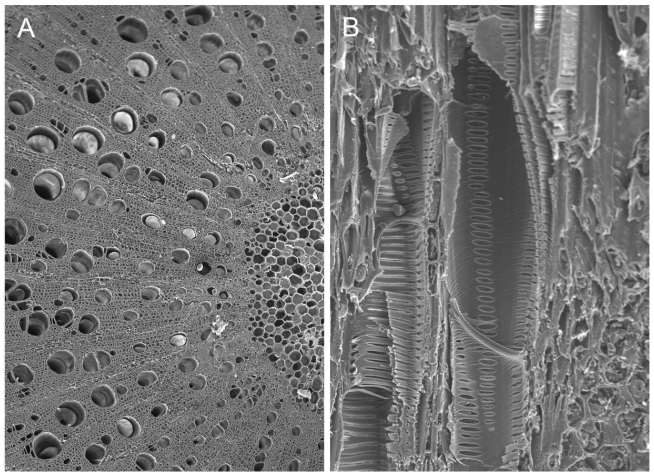

Figure 11: Xylem structural features in PBS-inoculated Cabernet Sauvignon vine at the late timepoint. **A.** Transverse section of stem secondary xylem, showing absence of occluded vessels. **B.** Longitudinal section of stem secondary xylem, showing vessels free of tyloses.

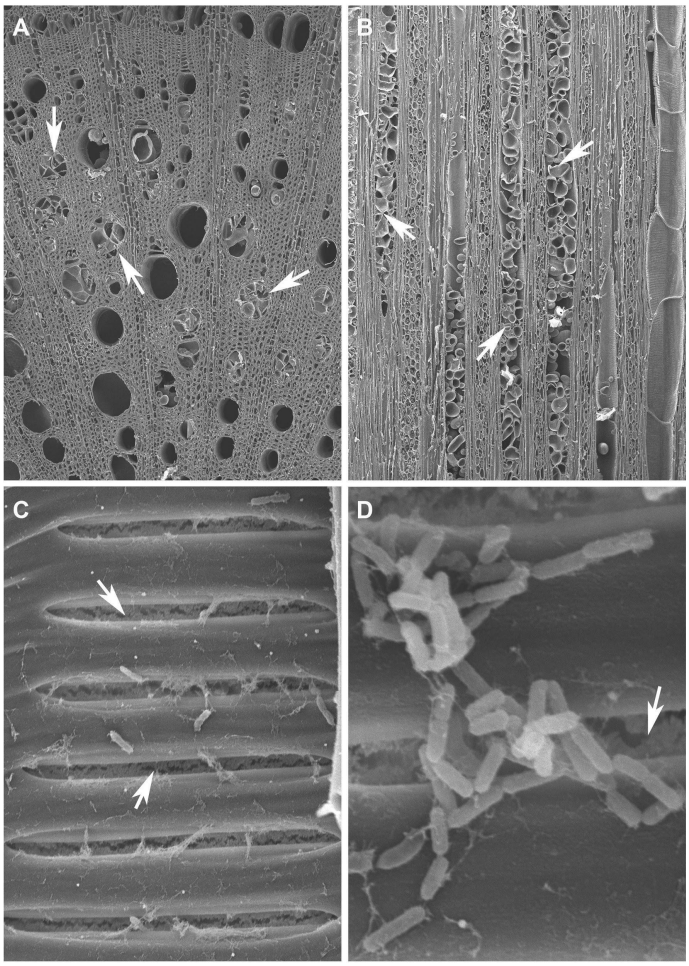

Figure 12: Xylem structural features in wild-type Temecula 1-inoculated Cabernet Sauvignon vine at the middle time-point. **A.** Transverse section of stem secondary xylem, showing a large number of vessels occluded (arrows). **B.** Tangential longitudinal section of secondary xylem, showing one empty vessel and three vessels completely occluded by tyloses (arrowed). **C.** A longitudinally transected vessel. Intervessel PMs are partially degraded (arrows) and wild-type Temecula 1 cells occur mostly individually. **D.** wild-type Temecula 1 cells occur as small clusters.

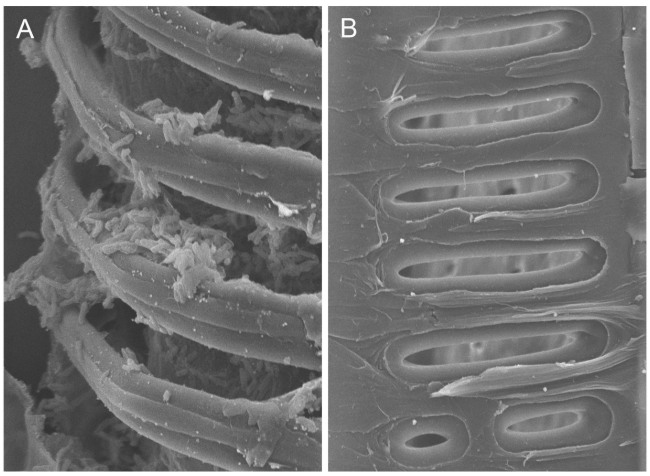

Figure 13: Xylem structural features in wild-type Temecula 1-inoculated Cabernet Sauvignon vine at the late time-point. **A.** Longitudinal section of stem secondary xylem, showing abundant presence of wild-type cells in a vessel. **B.** A longitudinally transected vessels, showing that intervessel PMs have completely disappeared.

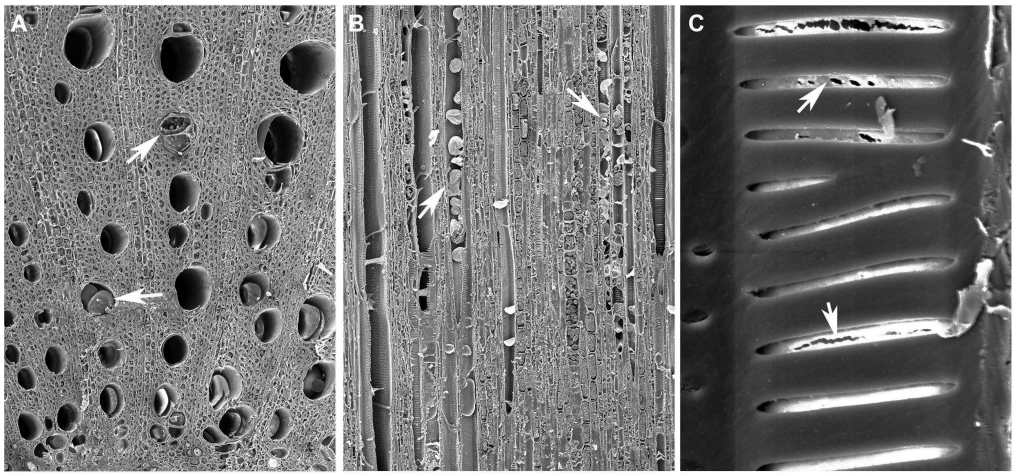

Figure 14: Xylem structural features in Δ*engXCA2*-inoculated Cabernet Sauvignon vine at the middle time-point of PD symptom development. **A.** Transverse section of stem secondary xylem. Few vessels are occluded (arrows). **B.** Longitudinal section of stem secondary xylem, showing two transected vessels fully occluded by tyloses. **C.** Broken intervessel PMs (arrows) and Δ*engXCA2* cells in a longitudinally transected vessel.

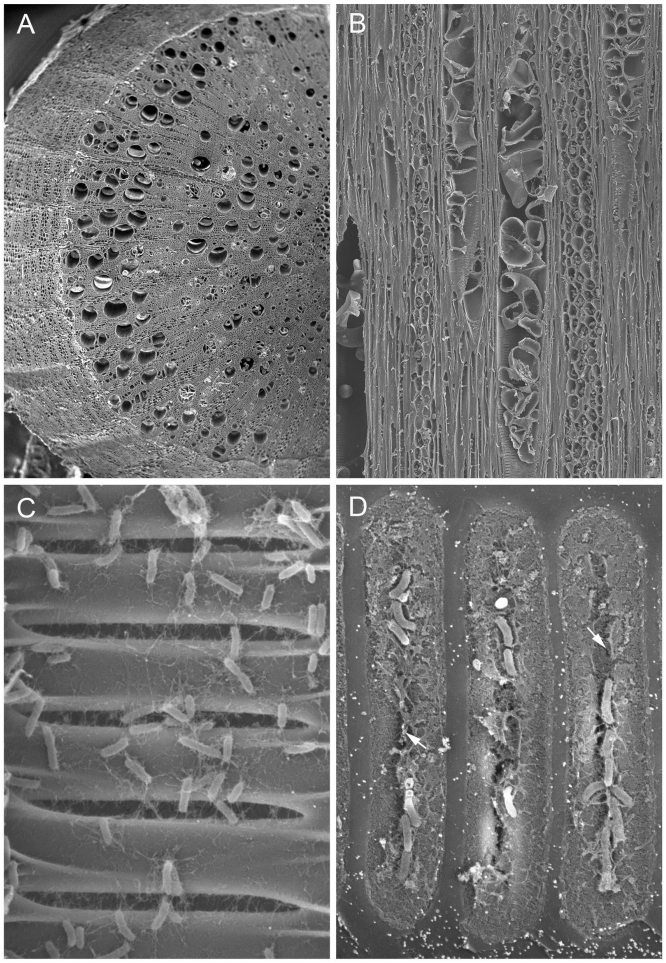

Figure 15: Xylem structural features in Δ*engXCA2*-inoculated Cabernet Sauvignon vine at the late time-point of PD symptom development. **A.** Transverse section of secondary xylem, showing occlusion in some vessels. **B.** Longitudinal section of secondary xylem, show two transected vessels fully occluded by tyloses. **C.** A longitudinally transected vessel, showing an abundant presence of Δ*engXCA2* cells. **D.** Δ*engXCA2* cells on partially some degraded intervessel PMs (arrows indicate pores or cracks in the PMs).

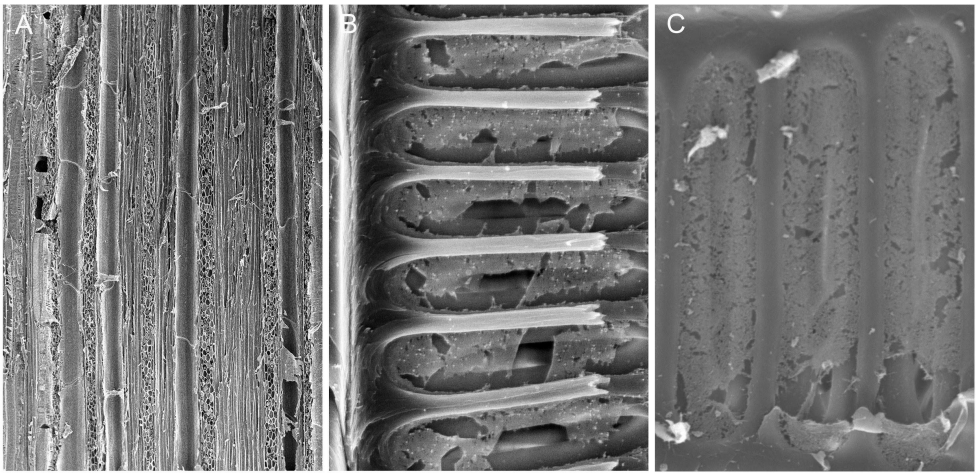

Figure 16: Xylem structural features in Δ*engXCA1*-inoculated Cabernet Sauvignon vine at the late timepoint of PD symptom development. **A.** Longitudinal section of stem secondary xylem, showing open vessels. **B** and **C.** Longitudinally transected vessels, showing intervessel PMs with large (B) and small (C) pores, respectively.

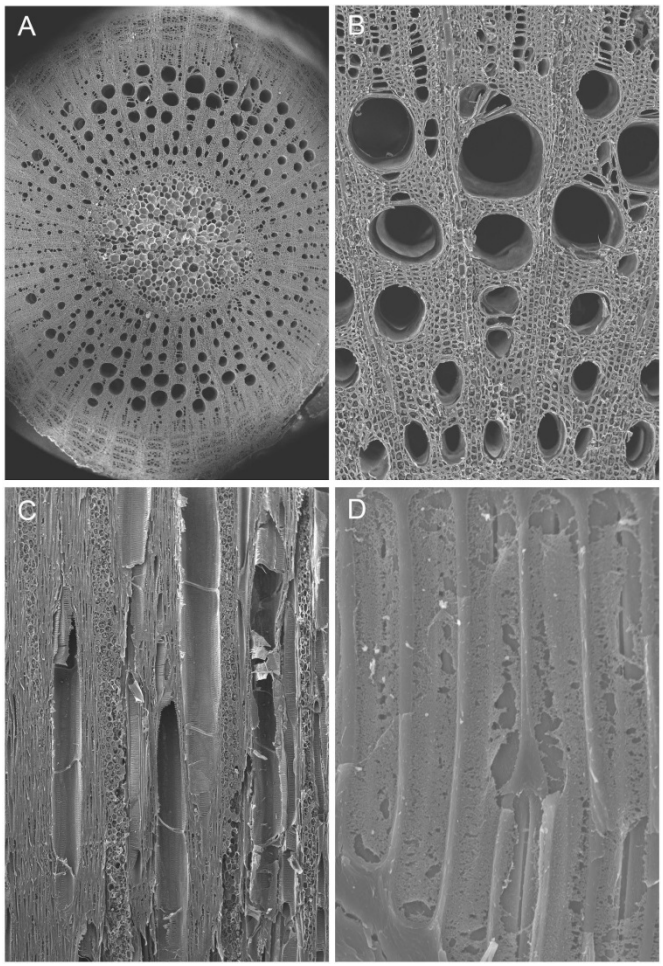

Figure 17: Xylem structural features in Δ*engXCA1*/Δ*engXCA2*-inoculated Cabernet Sauvignon vine at the late timepoint of PD symptom development. **A** and **B.** Transverse section of stem secondary xylem, showing vessels free of occlusions. **C.** Longitudinal section of secondary xylem, showing empty vessels with mostly intact PMs. **D.** A longitudinally transected vessel, showing pores of different sizes in intervessel PMs.

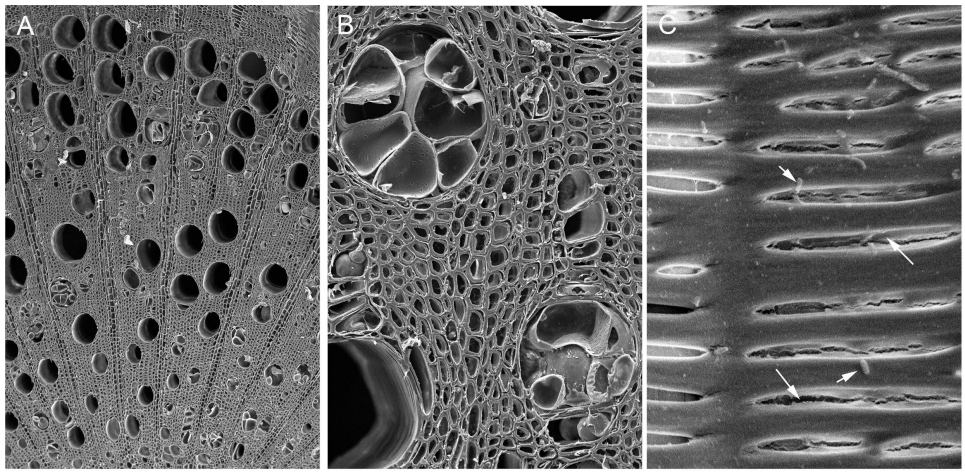

Figure 18: Xylem structural features in Δ*egl*-inoculated Cabernet Sauvignon vine at the late time-point of PD symptom development. **A** and **B.** Transverse section of stem secondary xylem, showing occurrence of vascular occlusion in some vessels (A) and fully occluded vessels (B). **C.** A longitudinally transected vessel, showing Δ*egl* cells (short arrows) and broken PMs (long arrows).

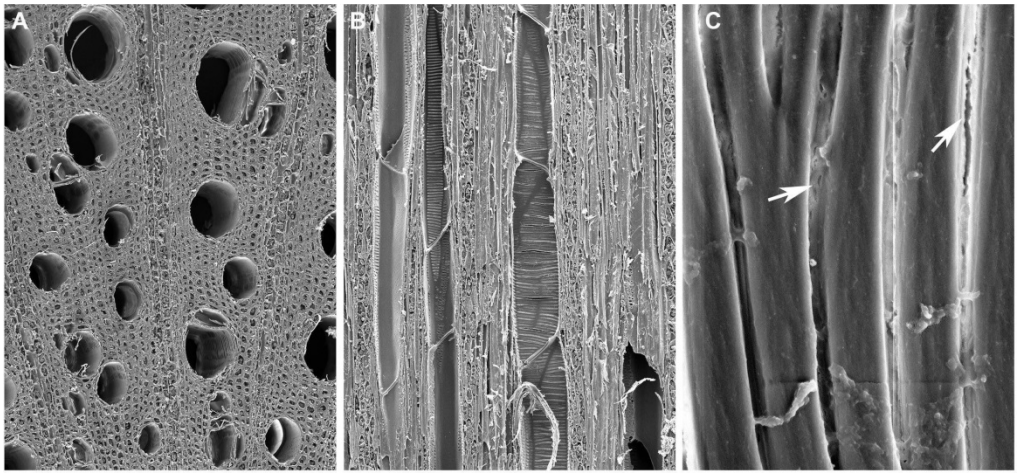

Figure 19: Xylem structural features in Δ*pglA*-inoculated Cabernet Sauvignon vines at the middle time-point of PD symptom development. **A.** Transverse section of secondary xylem, showing vessels are free of vascular occlusions. **B.** Tangential longitudinal section of secondary xylem, showing two transected vessels without tyloses. **C.** The surface view of intervessel PMs, showing that small pores and cracks on several PMs (arrows).

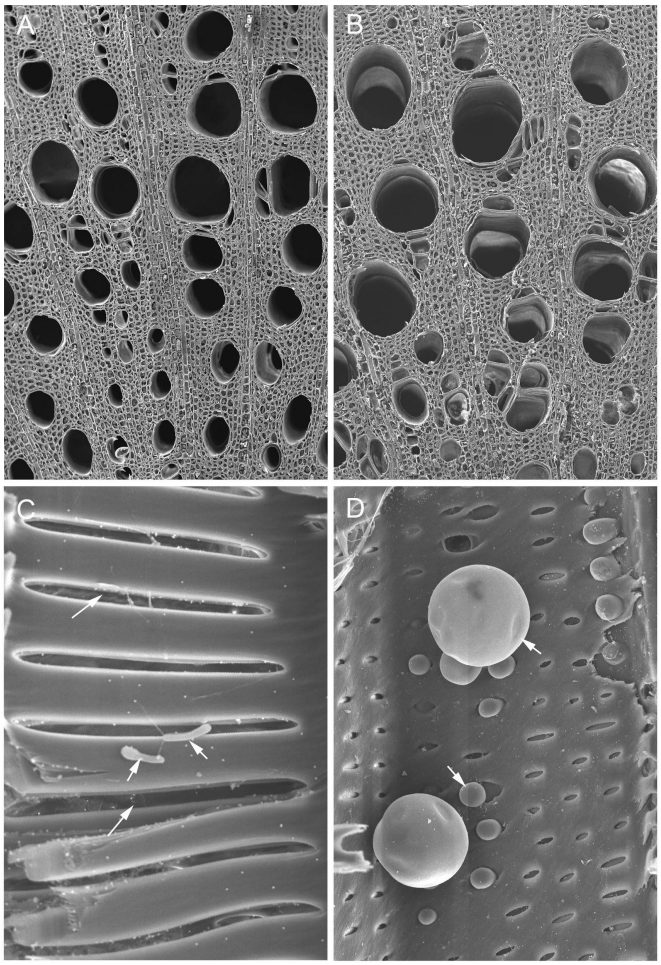

Figure 20: Xylem structural features in wild-type Fetzer (A, C, D)- and Δ*pglA* (B)-inoculated Cabernet Sauvignon vines at the late time-point of PD symptom development. **A** and **B.** Transverse section of stem secondary xylem, showing open vessels. **C.** A longitudinally transected vessel, showing broken intervessel PMs (long arrows) and Fetzer wild-type cells (short arrows). **D.** Small tyloses (arrows) are present in a longitudinal transected vessel.

In addition to samples imaged via electron microscopy, samples from the early and middle time-points in both Chardonnay and Cabernet Sauvignon have also been analyzed by microCT. This technique is particularly resource-intensive and thus, imaging all nine samples per treatment was not feasible. Instead, three samples per treatment were chosen randomly, and singular midslice images were analyzed to determine if tyloses formed in the xylem in response to *Xf* infection. Cabernet Sauvignon vines inoculated with wild-type Temecula 1 or Δ*engXCA2* exhibited the most blocked vessels by tyloses at all timepoints, whereas vines inoculated with Δ*engXCA1* exhibited fewer tyloses (Fig. 21). Additionally, vines inoculated with the wild type Fetzer strain and the *pglA* mutant exhibited very few tyloses, and vines inoculated with PBS (negative control) displayed no tyloses.

Transverse and longitudinal images slices of the selected samples from the early time-point in Chardonnay were also performed to visualize tylose formation, and machine learning algorithms were used to detect and quantify tyloses within vessels (Fig. 22). Several vessels from vines inoculated with wild-type Temecula 1 displayed tyloses, while fewer vessels were occluded in vines inoculated with the Δ*engXCA1* mutant (Fig. 23). Vessels from vines inoculated with the PBS negative control were occlusion-free and displayed no tylose formation.

The McElrone lab recently developed a method to measure starch content in ray and axial parenchyma (RAP) *in vivo* using microCT and machine learning algorithms (Earles 2018). In microCT images, x-ray absorption corresponds to the distinct molecular structure of air, water, starch and cell wall material, which enables the visualization of RAP, which are located in xylem tissue between radial files of vessels. While microCT images pictured here are of dried stems, patterns of full/empty RAP reflect those found *in vivo* in grapevine rootstocks and the method has implications for tracking starch utilization over the course of *Xf* infection. RAP in Cabernet Sauvignon vines inoculated with wild-type Temecula 1 show patterns of starch depletion at an early timepoint with significant depletion at a late timepoint, while RAP in Δ*engXCA1*-inoculated vines show RAP tissue full of starch at an early timepoint and moderate depletion at a late timepoint (Fig 24). RAP in PBS-inoculated vines remain full of starch at all timepoints. This technique is currently being used to analyze all samples for starch depletion.

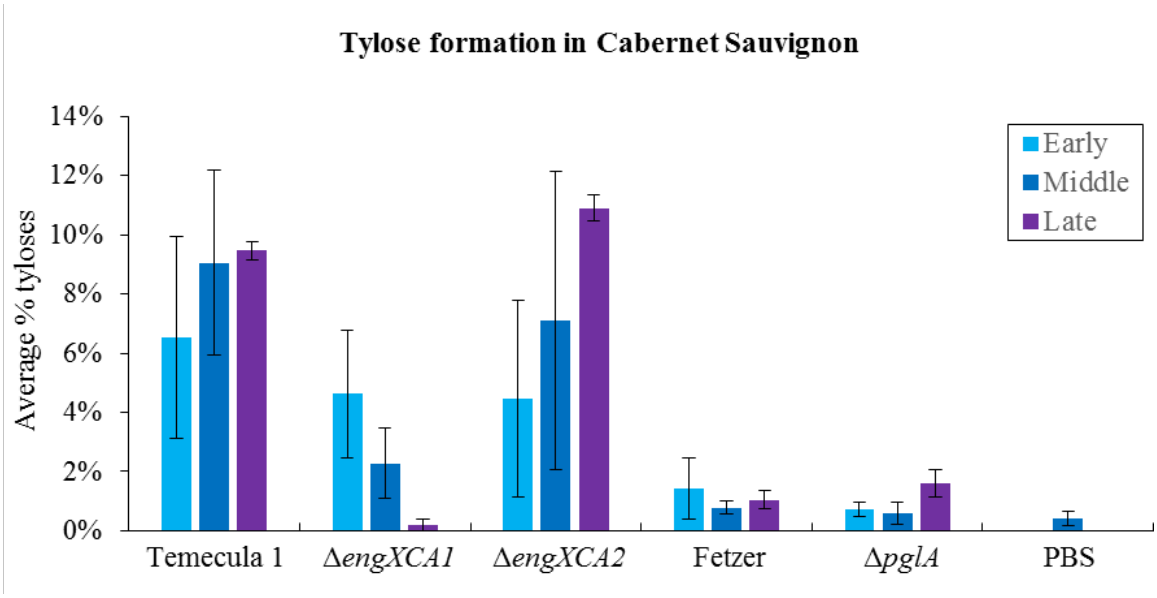

Figure 21: Manual midslice analysis of %-tyloses (occluded vessels/total vessels) per treatment in Cabernet Sauvignon. Vessels with tyloses were manually counted on midslices of microCT scans. wild-type Temecula 1 treatment showed high tylose formation relative to wild-type Fetzer. Δ*engXCA1* treatments exhibited less tyloses than wild-type Temecula 1 overall, and a reduction of occluded vessels from early to late timepoints. Δ*engXCA2* treatments show tyloses formation comparable to wild-type Temecula 1.

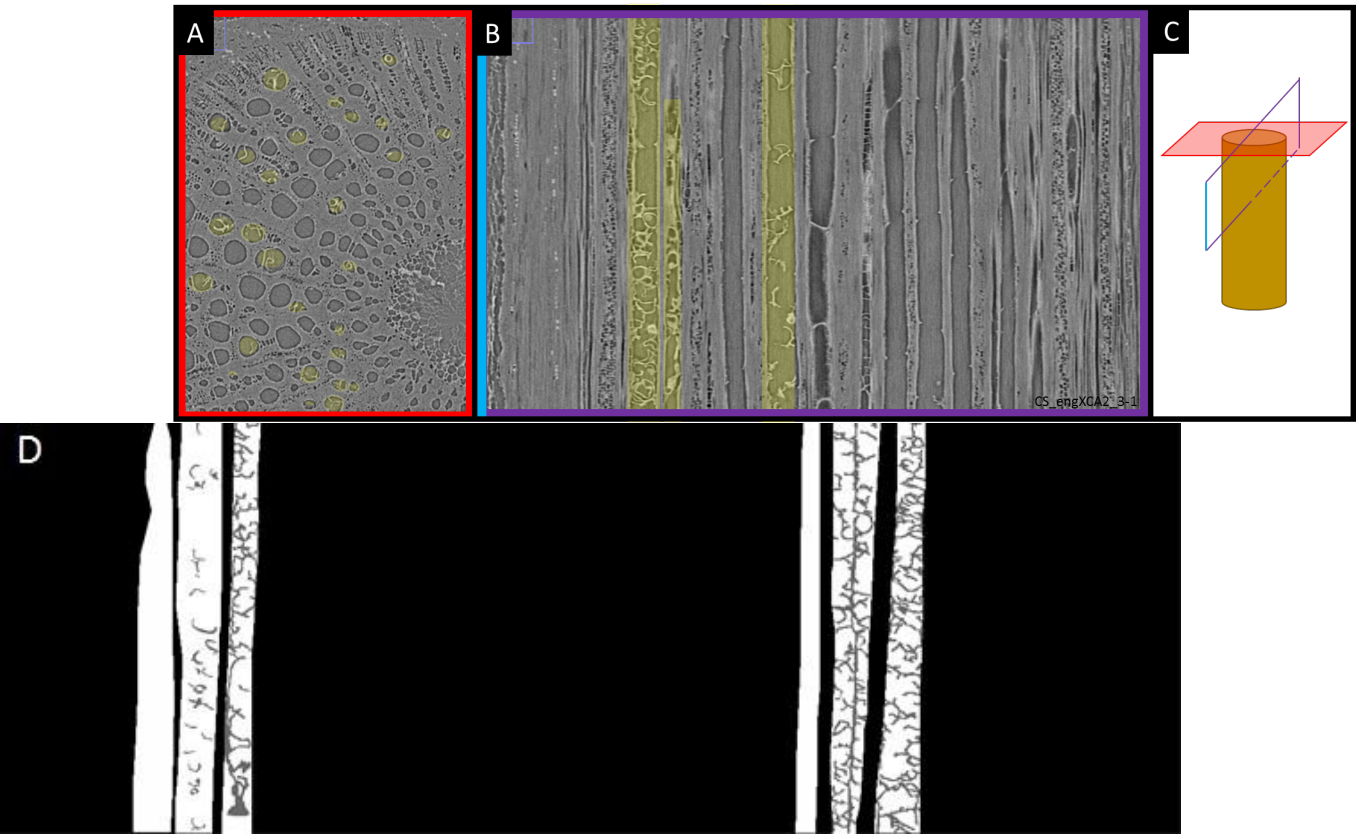

Figure 22: Improved tyloses detection/quantification. Colored outlines in **A** (xy-axis) and **B** (yz-axis) correspond with **C** to help orient the viewer. Tyloses (highlighted in yellow) are small and rare features relative to empty vessels on the xy-axis, and can easily be confused with interconnected vessels, yet appear more distinctly in the yz-axis. **D**, longitudinal slices on the yz-axis can be used to train machine learning algorithms to automatically classify vessels containing tyloses for high throughput analysis.

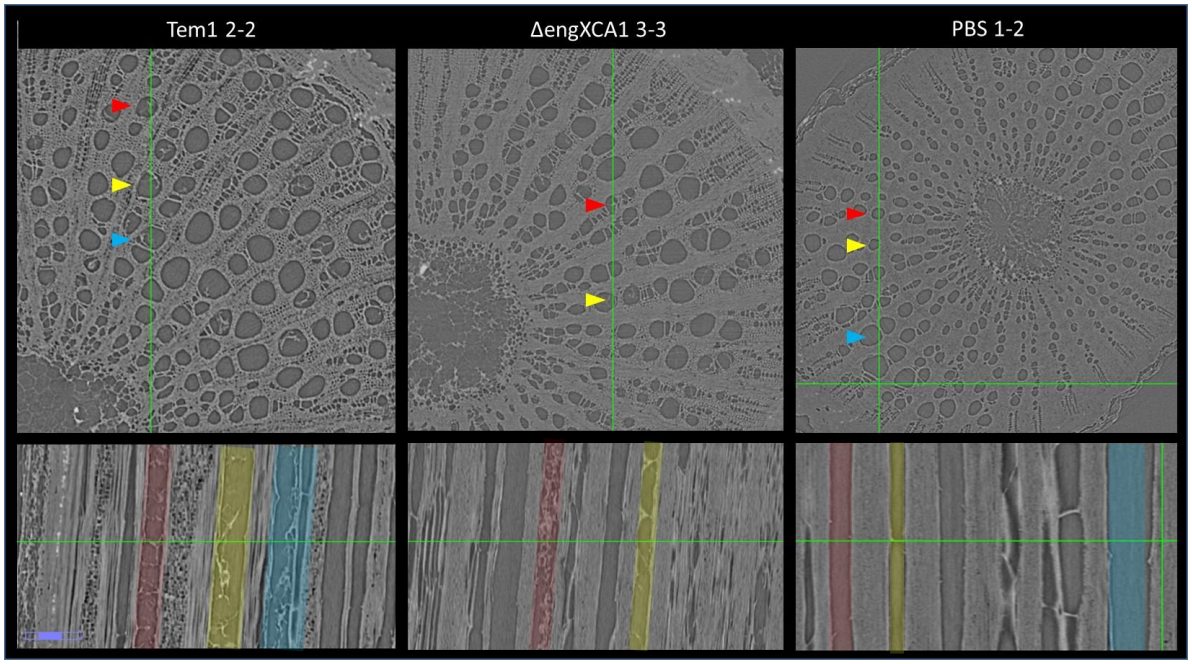

Figure 23: ImageJ orthogonal views of tyloses in Chardonnay (early timepoint) vines inoculated with wild-type Temecula 1, Δ*engXCA1*, or PBS (negative control). Colored arrows on tranverse image slices (top) correspond to highlighted vessels of same color on the longitudinal image slices (bottom), cut from the vertical green line in the transverse image. Empty vessels appear dark gray, while tyloses appear as highly branched membranes within vessel elements. PBS buffer treatment exhibits no tylose formation.

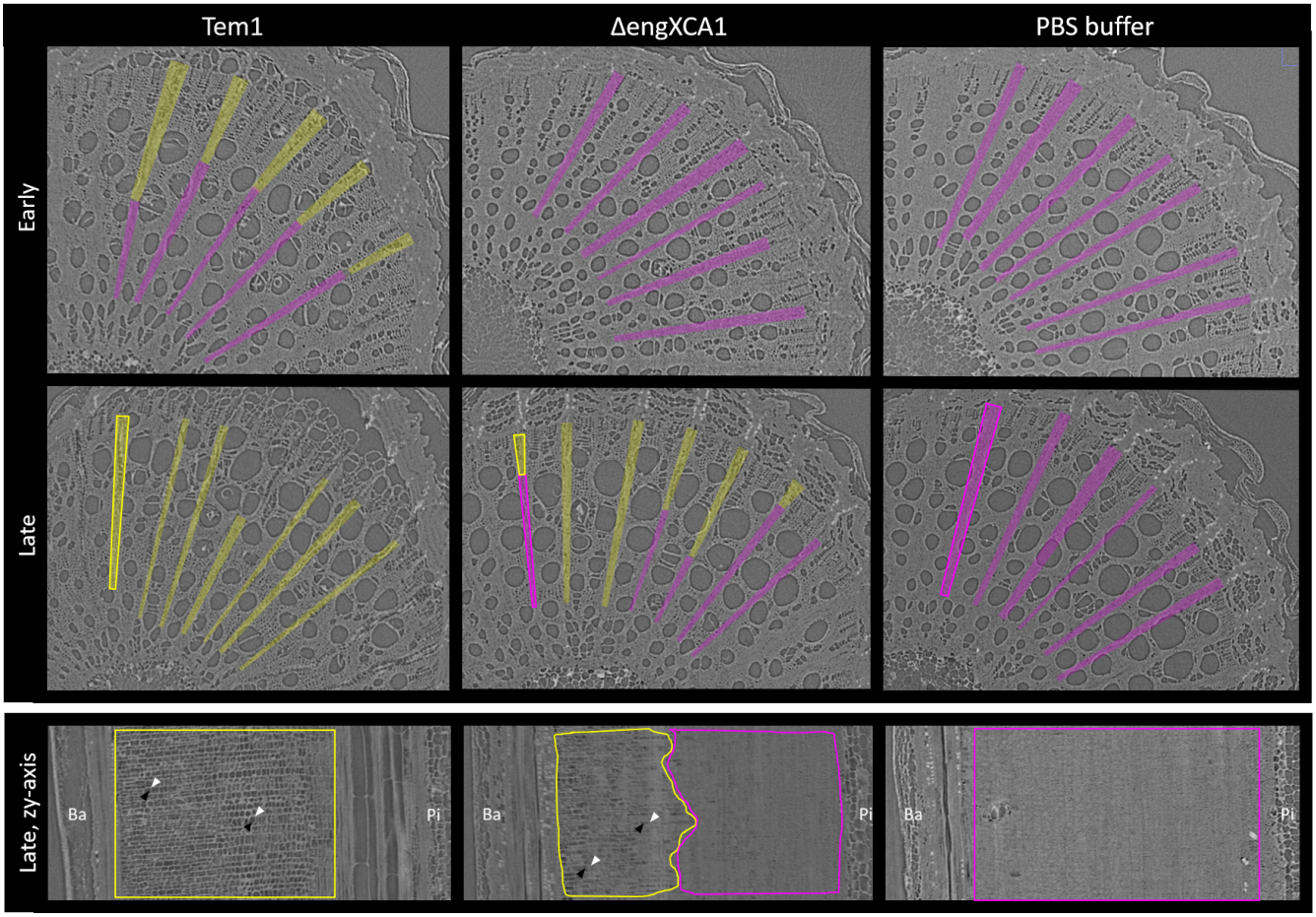

Figure 24: Visual classification of ray and axial parenchyma (RAP) regions as full (magenta) or empty (yellow) in Cabernet Sauvignon vines inoculated with either wild-type Temecula 1, Δ*engXCA1*, or PBS (negative control).. Longitudinal slices of outlined, late-timepoint RAP emphasize a spatial pattern of starch depletion with empty cells (dark airspace and light cell walls indicated with corresponding triangles) near the periphery bark (Ba) layer progressing towards the pith (Pi).

Quantitative analysis of plant defense pathways induced by *Xf* cell wall degrading enzyme activity: biochemical and transcriptional studies.

Pit membrane degradation by *Xf* CWDEs likely results in the release of small chain carbohydrates into the xylem. These oligosaccharides have been known to act as elicitors of plant immunity (i.e. damage-associated molecular patterns). It is possible that oligosaccharides released from pit membrane degradation are being recognized by associated parenchyma cells, triggering defense responses such as tylose production. To test this hypothesis, we used RNAseq to analyze the Cabernet Sauvignon transcriptome to determine if pit membrane degradation products act as elicitors of plant immunity and trigger tylose production. So far, we have counts of differentially expressed genes (DEGs, p-value < 0.05) from the early and middle time-points in 2016 and the early time-point in 2017. When compared to PBS-inoculated vines, the transcriptomes of vines inoculated with either wild-type *Xf* or any of the endoglucanase mutant strains differed significantly (Table 1). When compared to wild-type *Xf*-inoculated vines, the transcriptomes of all vines inoculated with any of the *Xf* endoglucanase mutant strains differed significantly, though there were less DEGs in Δ*engXCA1*- and Δ*engXCA2*-inoculated vines and more in Δ*engXCA1*/Δ*engXCA2*-inoculated vines (Table 2).

Table 1: Summary of the differentially expressed genes (DEGs; *P*-value < 0.05) between the Cabernet Sauvignon vines inoculated with *Xf* strains (wild-type, Δ*engXCA1*, Δ*engXCA2*, or Δ*engXCA1*/ Δ*engXCA2*) and PBS.

Year	Time point	Number of DEGs	Wild-type vs. PBS	Δ*engXCA1* vs. PBS	Δ*engXCA2* vs. PBS	Δ*engXCA1*/ Δ*engXCA2* vs. PBS
2016	Early	Up-regulated	2,831	2,335	469	-
		Down-regulated	1,805	1,446	240	-
		Total	4,636	3,781	709	-
	Middle	Up-regulated	1,791	4,495	1,263	-
		Down-regulated	471	2,566	325	-
		Total	2,262	7,061	1,588	-
2017	Early	Up-regulated	4,567	1,356	3,272	449
		Down-regulated	3,114	638	1,789	259
		Total	7,681	1,994	5,061	708

Table 2: Summary of the differentially expressed genes (DEGs; *P*-value < 0.05) between the Cabernet Sauvignon vines inoculated with the endoglucanase mutant strains and the wild-type *Xf* strain.

Year	Time point	Number of DEGs	Δ*engXCA1* vs. WT	Δ*engXCA2* vs. WT	Δ*engXCA1*/Δ*engXCA2* vs. WT
2016	Early	Up-regulated	215	1,214	-
		Down-regulated	260	1,695	-
		Total	475	2,909	-
	Middle	Up-regulated	486	29	-
		Down-regulated	255	89	-
		Total	741	118	-
2017	Early	Up-regulated	1,717	300	2,866
		Down-regulated	2,965	507	4,068
		Total	4,682	807	6,934

Inhibition of the Type II secretion system using natural products produced by grapevine microbial endophytes.

Given that *Xf* CWDEs are important for the degradation of pit membranes (thus allowing systemic colonization), and their potential role in inducing tylose formation, it is imperative that these virulence factors are targeted for inhibition. However, inhibiting each CWDE individually as a commercial strategy for controlling *Xf* is both impractical and costly. Interestingly, these CWDEs are predicted (using SignalP software) to be secreted via the Type II secretion system (T2SS). The T2SS is a molecular nanomachine that transports pre-folded proteins from the periplasm across a dedicated channel in the outer membrane (Cianciotto, 2005, Korotkov et al., 2012). The T2SS systems of many plant and animal pathogens are either known or predicted to secrete proteins, namely polymer degrading enzymes, which are involved in nutrient acquisition (Jha et al., 2005). The *Xf* CWDEs being studied in this proposal are predicted (using SignalP software) to be secreted through the T2SS. Proteins destined for secretion by the T2SS are first delivered to the periplasm via the Sec or Tat-dependent secretion pathway where they are folded (Slonczewski, 2014). *Xf* appears to only possess the Sec-dependent secretion pathway. Because of our interest in host CWDEs and their mechanism of secretion, we created a mutation in the *xpsE* gene, which encodes the putative ATPase that powers the T2SS**.** Grapevines inoculated with the *xpsE* mutant never developed PD symptoms and remained healthy, a phenotype similar to the grapevine response to the *Xf pglA* mutant (Fig. 25).

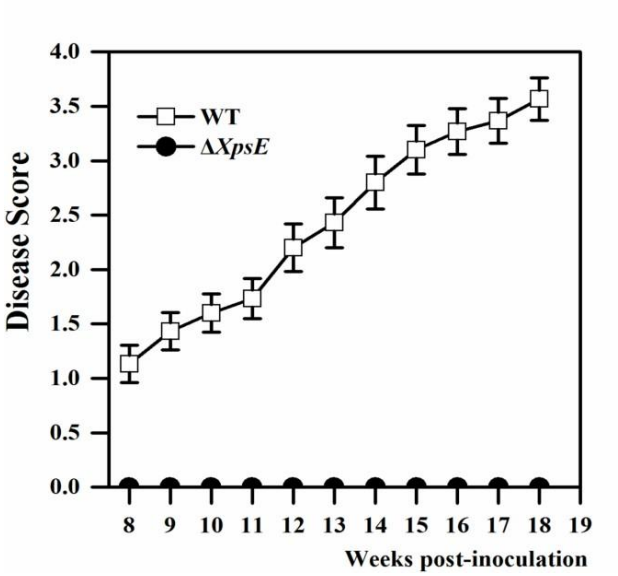

Figure 25: The *Xf* T2SS is necessary for PD development in grapevine. The Δ*xpsE* mutant does not induce PD symptoms in *V. vinifera* grapevines. Disease severity was based on a visual disease scale from 0 (no disease) to 5 (dead). Vines inoculated with 1X PBS (negative control) did not develop PD symptoms.

We hypothesize that this is due to the pathogen's inability to secrete the CWDEs necessary for xylem colonization. In addition, we have indirect experimental evidence that *Xf* utilizes the T2SS to secrete PG. We observed that the Δ*xpsE* mutant produces visibly less EPS on XFM minimal medium containing pectin as the sole carbon source, resulting in a much less mucoid phenotype (*data not shown).* However, when wild type *Xf* and Δ*xpsE* are grown on XFM+galacturonic acid (i.e., the monomeric sugar that makes up the pectin polymer) or on XFM+glucose, both strains produce similar amounts of EPS. We infer from this that, indeed, breakdown of the pectin substrate is necessary to produce EPS and when the T2SS is disrupted this prevents secretion of PG and the subsequent breakdown of pectin.

Thus, we have compelling *in planta* and *in vitro* preliminary data indicating that *Xf* has a functional T2SS system and the proteins secreted by T2SS are critical for the infection process. From this we reason that the T2SS represents an excellent target for disease control because disrupting this system would provide comprehensive inhibition of secretion of PG (the major pathogenicity factor for *Xf*) and the other auxiliary CWDEs (Roper et al. 2007 and recent results discussed above). Therefore, identifying molecules that can inhibit T2SS function is an excellent avenue of research to pursue to develop strategies that mitigate PD by preventing pathogen ingress. This work is ongoing.

PUBLICATIONS AND PRESENTATIONS

Poster Presentations

Brian M. Ingel, Dario Cantu, Andrew McElrone, Qiang Sun, John Labavitch, and M. Caroline Roper. Characterization of *Xylella fastidiosa* plant cell wall degradation and inhibition of the Type II secretion machinery (2016). Pierce's Disease Research Symposium, San Diego, CA.

Brian M. Ingel, Andrew McElrone, Qiang Sun, Dario Cantu, Daniel Jeske, M. Caroline Roper. Characterization of Xylella fastidiosa plant cell wall degradation and inhibition of the Type II secretion machinery (2018). Pierce's Disease Research Symposium, San Diego, CA.

RESEARCH RELEVANCE STATEMENT

Xf is the causal agent of PD of grapevine, a serious and often lethal disease of grapevines (Hopkins and Purcell, 2002, Chatterjee et al., 2008, Purcell and Hopkins, 1996). This xylem-limited bacterial pathogen colonizes the xylem and in doing so must be able to move efficiently from one xylem vessel element to adjacent vessels (Roper et al. 2007). Xylem conduits are separated by pit membranes (PMs) that are composed of primary cell wall that serve to prevent movement of air embolisms and pathogens within the xylem (Buchanan, 2000). More specifically, PMs are composed of cellulose microfibrils embedded in a meshwork of pectin and hemicellulose (Buchanan, 2000). The pore sizes within that meshwork range from 5 to 20 nM, which will not allow passive passage of *Xf* cells whose size is 250-500 x 1,000-4,000 nM (Perez-Donoso et al., 2010, Mollenhauer & Hopkins, 1974). Based on functional genomics and *in planta* experimental evidence, *Xf* utilizes host CWDEs to actively digest the polymers within the PMs, thereby facilitating its movement throughout the xylem network (Roper et al., 2007, Perez-Donoso et al., 2010). This previous work demonstrated that a polygalacturonase (PG), PglA, was required for movement and pathogenicity in grape (Roper et al, 2007). In addition, an EGase (EngXCA2) worked in concert with PG to breach pit membranes (Perez-Donoso et al. 2010). Based on these findings, inhibition of *Xf* PG has been identified as a top research priority by the PD research board. Several other research groups are working towards inhibiting PG *in planta* as a means of PD control. In our currently supported project (project # 14-0144-SA), we have outlined objectives designed to complement and augment these current research efforts that are aimed at inhibiting PG. Our central hypothesis is that *Xf* utilizes other CWDEs in concert with PG to breach the pit membranes and that the majority of these are secreted by a common mechanism, the Type II Secretion System (T2SS). Our project is composed of two broad goals: 1) Elucidation of how the plant perceives host cell wall damage inflicted by the suite of *Xf* CWDEs during the infection process and 2) Utilization of natural products produced by grapevine microbial endophytes to inhibit the T2SS that delivers PG, and other CWDEs (EGases) to the xylem. We view this as a comprehensive approach to achieving disease control with the potential impact being to effectively disrupt systemic spread of *Xf* and vascular occlusions in the xylem and, therefore, PD development.

LAYPERSON SUMMARY

Xylella fastidiosa (*Xf*) relies on degradation of the plant cell wall to move within the grapevine, which occurs through cooperation between at least two classes of enzymes that target different carbohydrate components of the complex scaffold of the plant cell wall. A major goal of this project is to elucidate the mechanisms that lead to disassembly of the plant cell wall that eventually leads to systemic colonization of *Xf* in grapevines. Here we are performing experiments designed to better understand what facilitates movement of the bacterium and the subsequent clogging of the water-conducting cells that worsens Pierce's Disease severity. In addition, we also are designing experiments to inhibit the secretion machinery responsible for delivering the *Xf* enzymes that are involved in *Xf* movement throughout the plant, thus, providing a comprehensive approach to restriction of *Xf* and disease development rather than targeting individual enzymes.

STATUS OF FUNDS

The funding for this project is largely going towards supporting a Ph.D. graduate student, Mr. Brian Ingel. This project is the main focus of his Ph.D. dissertation. We anticipate spending the remainder of the salary, supply, services and greenhouse recharge money associated with this project as it progresses.

SUMMARY AND STATUS OF INTELLECTUAL PROPERTY

There is no intellectual property associated with this project to date.

REFERENCES

Aleemullah M, Walsh KB (1996) Australian papaya dieback: Evidence against the calcium deficiency hypothesis and observations on the significance of laticifer autofluorescence. Australian Journal of Agricultural Research 47: 371-385

Benedetti M, Pontiggia D, Raggi S*, et al.*, 2015. Plant immunity triggered by engineered in vivo release of oligogalacturonides, damage-associated molecular patterns. *Proc Natl Acad Sci U S A* **112**, 5533-8.

Boller T, Felix G, 2009. A renaissance of elicitors: perception of microbe-associated molecular patterns and danger signals by pattern-recognition receptors. *Annu Rev Plant Biol* **60**, 379-406.

Bonsen KJM, Kučera LJ (1990) Vessel occlusions in plants: morphological functional and evolutionary aspects.

International Association of Wood Anatomists Bulletin 11: 393-399
Buchanan BB, Gruissem, W., and Jones, R.L. , 2000. Biochemistry and Molecular Biology of Plants. *American Society of Plant Physiologists. Maryland.* **Chapter 2: The Cell Wall**, 52-100.

Chatterjee S, Almeida RPP, Lindow S, 2008. Living in two worlds: The plant and insect lifestyles of *Xylella fastidiosa*. *Annual Review of Phytopathology* **46**, 243-71.
Cianciotto NP, 2005. Type II secretion: a protein secretion system for all seasons. *Trends Microbiol* **13**, 581-8.
Collins BR, Parke JL, Lachenbruch B, Hansen EM (2009) The effects of Phytophthora ramorum infection on hydraulic conductivity and tylosis formation in tanoak sapwood. Canadian Journal of Forest Research- Revue Canadienne De Recherche Forestiere 39: 1766-1776
Dimond AE (1955) Pathogenesis in the Wilt Diseases. Annual Review of Plant Physiology and Plant Molecular Biology 6: 329-350
Earles, J. M., Knipfer, T., Tixier, A., Orozco, J., Reyes, C., Zwieniecki, M. A., ... & McElrone, A. J. (2018). In vivo quantification of plant starch reserves at micrometer resolution using X1ray microCT imaging and machine learning. *New Phytologist*.
Esau K (1977) Anatomy of Seed Plants. 2nd edition. Wiley, New York, NY
Fritschi FB, Lin H, Walker MA (2008) Scanning electron Microscopy reveals different response pattern of four Vitis genotypes to Xylella fastidiosa infection. Plant Disease 92: 276-286
Gough CL, Dow, M.J., Barber, C.E. And Daniels, M.J., 1988. Cloning of two endoglucanase genes of *Xanthomonas campestris* pv. *campestris*: analysis of the role of the major endoglucanase in pathogenesis. *Molecular Plant Microbe Interactions* **1**, 275-81.
Guilhabert MR, Kirkpatrick BC, 2005. Identification of *Xylella fastidiosa* antivirulence genes: hemagglutinin adhesins contribute to *X. fastidiosa* biofilm maturation and colonization and attenuate virulence. *Molecular Plant-Microbe Interactions* **18**, 856-868.
Hopkins DL, Purcell AH, 2002. *Xylella fastidiosa*: Cause of Pierce's disease of grapevine and other emergent diseases. *Plant Disease* **86**, 1056-66.
Jha G, Rajeshwari R, Sonti RV, 2005. Bacterial type two secretion system secreted proteins: double-edged swords for plant pathogens. *Molecular Plant Microbe Interactions* **18**, 891-8.
Korotkov KV, Sandkvist M, Hol WG, 2012. The type II secretion system: biogenesis, molecular architecture and mechanism. *Nature Reviews Microbiology* **10**, 336-51.
Mohammadi M, Burbank L, Roper MC, 2012. *Pantoea stewartii* subsp. *stewartii* produces an endoglucanase that is required for full virulence in sweet corn. *Molecular Plant Microbe Interactions* **25**, 463-70.
Mollenhauer HH, Hopkins DL, 1974. Ultrastructural study of Pierce's disease bacterium in grape xylem tissue. *J Bacteriol* **119**, 612-8.
Parameswaran N, Knigge H, Liese W (1985) Electron microscopic demonstration of a suberized layer in the tylosis wall of beech Fagus sylvatica and oak Quercus robur. International Association of Wood Anatomists Bulletin 6: 269-271
Parke JL, Oh E, Voelker S, Hansen EM, Buckles G, Lachenbruch B (2007) Phytophthora ramorum colonizes tanoak xylem and is associated with reduced stem water transport. Phytopathology 97: 1558-1567
Perez-Donoso AG, Sun Q, Roper MC, Greve LC, Kirkpatrick B, Labavitch JM, 2010. Cell Wall-Degrading Enzymes Enlarge the Pore Size of Intervessel Pit Membranes in Healthy and Xylella fastidiosa-Infected Grapevines. *Plant Physiology* **152**, 1748-59.
Purcell AH, Hopkins DL, 1996. Fastidious xylem-limited bacterial plant pathogens. *Annu Rev Phytopathol* **34**, 131-51.
Roberts DP, Denny TP, Schell MA, 1988. Cloning of the egl gene of *Pseudomonas solanacearum* and analysis of its role in phytopathogenicity. *J Bacteriol* **170**, 1445-51.
Roper MC, Greve LC, Warren JG, Labavitch JM, Kirkpatrick BC, 2007. Xylella fastidiosa requires polygalacturonase for colonization and pathogenicity in Vitis vinifera grapevines. *Molecular Plant Microbe Interactions* **20**, 411-9.
Saile E, Mcgarvey JA, Schell MA, Denny TP, 1997. Role of Extracellular Polysaccharide and Endoglucanase in Root Invasion and Colonization of Tomato Plants by Ralstonia solanacearum. *Phytopathology* **87**, 1264- 71.
Simpson AJ, Reinach FC, Arruda P*, et al.*, 2000. The genome sequence of the plant pathogen *Xylella fastidiosa*. The Xylella fastidiosa Consortium of the Organization for Nucleotide Sequencing and Analysis. *Nature* **406**, 151-9.
Slonczewski J.L. and Foster, J.W., 2014. Microbiology: An Evolving Science. *W.W. Norton and Company, New*

York, NY.
Sun. Q., Sun. Y., Juzenas, K. 2017. Immunogold scanning electron microscopy can reveal the polysaccharide architecture of xylem cell walls. *Journal of Experimental Botany* **68**, 2231-2244.
Sun Q, Sun Y, Walker MA, Labavitch JM, 2013. Vascular occlusions in grapevines with Pierce's disease make disease symptom development worse. *Plant Physiol* **161**, 1529-41.
Tyree MT, Zimmermann MH (2002) Xylem Structure and The Ascent of Sap. 2nd Edition. Springer, Berlin, Germany

FUNDING AGENCIES
Funding for this project was provided by the CDFA Pierce's Disease and Glassy-winged Sharpshooter Board.